# Tidal deformabilities and radii of strange quark stars

Bo-Lin Li,[1,*] Yan Yan,[2,†] and Jia-Lun Ping[1,‡]

[1]*Department of Physics, Nanjing Normal University, Nanjing 210023, China*

[2]*School of Mathematics and Physics, Changzhou University, Changzhou, Jiangsu 213164, China*

(Received 26 January 2021; accepted 30 June 2021; published 2 August 2021)

The tidal deformabilities and radii of strange quark stars are studied via the quasiparticle model which includes the nonperturbative features of QCD in the low-density region. The results show that the mass constraint of $M_{\rm TOV} > 2.0\ M_\odot$ rules out the EOSs which are soft at low densities, while the constraint on the tidal deformability of $\Lambda_{1.4} < 800$ from GW170817 rules out the EOSs which are too stiff in the low density region. The range for the radius of a 1.4 $M_\odot$ strange quark star is 11.12 km $< R_{1.4} <$ 11.98 km. $\Lambda_{1.4}$ has a strong correlation with $R_{1.4}$, and the empirical correlation function is $\Lambda_{1.4} = 2.86 \times 10^{-5}(R/\mathrm{km})^{6.92}$, which is larger than that for neutron stars. The lower bound of $\Lambda_{1.4} > 513.66$ is also obtained. $\tilde{\Lambda}$ is a monotonically increasing function of the mass ratio $\eta$, but the slope is very small. And we conclude that the range of $\tilde{\Lambda}$ for GW190425 is $184.81 < \tilde{\Lambda} < 320.08$.

DOI: 10.1103/PhysRevD.104.043002

## I. INTRODUCTION

In order to study the properties of strange quark stars, such as the mass-radius relation and the correlation between tidal deformablity and radius (or mass), an equation of state (EOS) for strange quark matter should be specified. The latter describes the relation between the pressure and the energy density in strange quark matter.

In the center of strange quark stars, the baryon number density $n_B$ reaches $(4 \sim 7)n_0$, where $n_0$ is the nuclear saturation density and $n_0 \simeq 0.16$ nucleons per fm$^3$ [1], a range of densities which even the terrestrial heavy-ion experiments cannot access. Since quantum chromodynamics (QCD) has complicated nonperturbative effects in the low energy region, perturbative QCD (pQCD) calculations are valid only for $n_B \gtrsim (10 \sim 100)n_0$. Moreover, due to the sign problem, lattice QCD cannot calculate the EOS at finite chemical potential and zero temperature, either. Therefore, at present, it is still a big challenge to get the exact EOS of strange quark matter from the first principles of QCD. Hence, many phenomenological models that incorporate some basic features of QCD are commonly used in studying strange quark matter at finite chemical potential and temperature [2–6].

In this paper, the quasiparticle model which has been widely used to simulate the properties of the quark-gluon plasma (QGP) at finite temperature ($T$) and chemical potential ($\mu$) [7–9] is adopted to produce the EOS for strange quark matter at finite chemical potential and zero temperature. Then, we choose the mass constraint of $M_{\rm TOV} > 2.0\ M_\odot$ that comes from the observations of the pulsars PSR J0348 + 0432 ($m = 2.01 \pm 0.04 m_\odot$) [10] and PSR J1614-2230 ($m = 1.928 \pm 0.017 m_\odot$) [11] and the tidal deformablity constraint of $\Lambda_{1.4} < 800$ that is obtained from the direct detection of the gravitational wave (GW) originated from a binary system inspiral by LIGO and Virgo network [12] to analyze the features of astrophysically compatible EOSs, the mass-radius relations, the correlation between tidal deformablity and radius, and the combined tidal deformablities for the cases of GW170817 and GW190425. The results present some interesting features of strange quark stars, which are evidently different from that of neutron stars.

This paper is organized as follows: In Sec. II, we give an introduction to the quasiparticle model and present the formula of the EOS for strange quark matter. Under the mass and tidal deformablity constraints, the results of mass-radius relations, the correlation between the tidal deformabilities and the radii for 1.4 $M_\odot$ strange quarks, and $\tilde{\Lambda}$ for GW170817 and GW190425 have been exhibited in detail in Sec. III. Finally, we give a summary of this work in Sec. IV.

## II. THE QUASIPARTICLE MODEL

In this section, we will introduce a nonperturbative method, the quasiparticle model, to describe the microscopic interaction between quarks and gluons, and finally to obtain the formula for the equation of state of strange quark matter. The formulas in this section are given in natural units.

The quasiparticle model provides a phenomenological method to study the thermodynamic properties of

*blli@njnu.edu.cn
†2919ywhhxh@163.com
‡jlping@njnu.edu.cn

 

QGP [13,14]. In recent years, explicit analytic expression for the EOS at zero temperature and finite chemical potential by means of the path integral method with an effective quark propagator was obtained [15,16]. In this paper, we follow the work in Refs. [15,16] and use the coupling $g$ obtained in the two loop approximation to construct the EOS of strange quark matter.

Assuming to know the full quark propagator at zero temperature $T$ and finite chemical potential $\mu$, the quark number density can be obtained via [15],

$$\rho_f(\mu) = -N_c \int \frac{\mathrm{d}^4 p}{(2\pi)^4} \mathrm{tr}_D\{\gamma_4 S_f(p,\mu)\}, \tag{1}$$

where $S_f(p,\mu)$ is the full quark propagator, $N_c$ is the number of colors which is given by $N_c = 3$, and the trace operator "$\mathrm{tr_D}$" is taken over all Dirac indices. Unfortunately, till now, the exact form of the full quark propagator at finite chemical potential $\mu$ and zero $T$ is still unknown from the first principles of QCD. Hence, an effective quark propagator that has the same form as the free quark propagator but with a density dependent effective quark mass is used as an approximation of the full quark propagator in the dense matter. Here, we take the form of the effective quark propagator proposed in [16],

$$S_f(p,\mu) = \frac{1}{i\gamma\cdot\tilde{p} + m_f(\mu)}, \tag{2}$$

where $\tilde{p} \equiv (\boldsymbol{p}, p_4 + i\mu)$ is the four momenta of the quark at finite $\mu$, and in Euclidean space, the gamma matrices satisfy $\{\gamma_\mu, \gamma_\nu\} = 2\delta_{\mu\nu}$. The effective quark mass which depends on $\mu$ reads [7,17,18],

$$m_f^2(\mu) = (m_{f0} + m_q(\mu))^2 + m_q^2(\mu), \tag{3}$$

with

$$m_q^2(\mu) = \frac{N_f \mu^2 g^2(\mu)}{18\pi^2}, \tag{4}$$

where $m_{f0}$ is the mass of current quark ($u$, $d$, or $s$), $N_f$ is the number of quark flavors which is given by $N_f = 3$, and $g(\mu^2)$ is the effective coupling constant obtained in the two loop approximation [19,20],

$$\alpha_s(\mu) = \frac{g^2(\mu)}{4\pi} = \frac{6\pi}{(33-2N_f)\ln(a\mu)}\left[1 - \frac{3(153-19N_f)}{(33-2N_f)^2}\frac{\ln(2\ln(a\mu))}{\ln(a\mu)}\right], \tag{5}$$

where $a = 1.91/(2.91\zeta)$, and $\zeta$ is a phenomenological parameter of the quasiparticle model, which characterizes the strength of the nonperturbative effect.

With the full quark propagator specified and using the contour integration method [21], we can obtain the quark number density for each quark flavor

$$\rho_f(\mu) = \frac{N_c}{3\pi^2}(\mu^2 - m_f^2(\mu))^{3/2}\theta(\mu - m_f(\mu)). \tag{6}$$

Since there is a step function on the right-hand side of Eq. (6), it is obvious that the quark number density will vanish when the quark chemical potential $\mu$ is smaller than a critical value $\mu_c$. This phenomenon qualitatively agrees with the general conclusions in Ref. [22]. In this model, the critical value depends on the current quark mass $m_{f0}$ and the parameter $\zeta$. In the case of chiral limit where the masses vanish, i.e., $m_{f0} = 0$, the critical value is given by $\mu_c \doteq 2.23\zeta$.

Then, according to Refs. [21,23], the pressure of the quark matter at finite $\mu$ and zero $T$ can be written as,

$$P(\mu) = P(\mu)|_{\mu=0} + \int_0^\mu \mathrm{d}\mu' \rho(\mu'), \tag{7}$$

where $P(\mu)|_{\mu=0}$ is the pressure at $\mu = 0$, which represents the vacuum pressure. Here we can rewrite it as $P(\mu)|_{\mu=0} \equiv -B(B > 0)$, where $B$ is also a phenomenological parameter in the present model. Please note that the parameter $B$ is a positive number, since we treat it as the bag constant in the MIT bag model. The vacuum pressure must be negative, which preserves the confinement of quarks. It should be also noticed that Eq. (7) is a model independent formula, for the pressure $P(\mu)$ at finite $\mu$ and zero $T$ can be determined by the quark number density $\rho(\mu)$ (up to a constant $P(\mu)|_{\mu=0}$). Therefore, assuming to know the quark number density $\rho(\mu)$ that matches the phenomena of QCD, one can obtain the pressure that satisfies the behavior of QCD at finite chemical potential $\mu$ and zero temperature $T$.

In strange quark stars, there are $u$, $d$, $s$ quarks in the system, and the baryon number density is defined by,

$$\rho_B(\mu) \equiv \frac{1}{3}(\rho_u(\mu_u) + \rho_d(\mu_d) + \rho_s(\mu_s)), \tag{8}$$

and the pressure of such system is given by,

$$P(\mu) = -B + P_u(\mu_u) + P_d(\mu_d) + P_s(\mu_s) + P_e(\mu_e). \tag{9}$$

Taking into account the electroweak interactions, we should take the constraints of chemical equilibrium and charge neutrality conditions,

$$\mu_d = \mu_u + \mu_e, \tag{10}$$

$$\mu_s = \mu_u + \mu_e, \tag{11}$$

$$\frac{2}{3}\rho_u = \frac{1}{3}\rho_s + \frac{1}{3}\rho_d + \rho_e, \tag{12}$$

where the number density of electrons at zero temperature is given by [24],

$$\rho_e(\mu_e) = \frac{\mu_e^3}{3\pi^2}. \tag{13}$$

Due to the constraints given by Eqs. (10), (11), and (12), there is only one independent chemical potential left. Here, we choose $\mu_u$, and the other chemical potentials, namely $\mu_d$, $\mu_s$, and $\mu_e$, can be treated as a function of $\mu_u$.

Finally, the energy density of the model is given by

$$\epsilon = -P + \mu \cdot \frac{\partial P}{\partial \mu} = -P + \sum_{f=u,d,s,e} \mu_f \rho_f(\mu_f). \tag{14}$$

As we can see from Eq. (14), the EOS constructed from the quasiparticle model depends on the masses of current quarks, the parameter $\zeta$, and the vacuum pressure $B$.

## III. TIDAL DEFORMABILITIES AND RADII OF STRANGE QUARK STARS

After the EOS of strange quark matter is established, it is now straightforward to explore the properties of strange quark stars. The formulas in this section are expressed in geometric units where $G = c = 1$. We will follow the perturbation scheme developed in Refs. [25–28] to compute the $l = 2$ dimensionless tidal Love number $k_2$ and the associated tidal deformalbility $\Lambda$. The tidal Love number describes how easily a substantial part of a star is deformed by an external tidal field, as discussed in Refs. [26,29,30], and $k_2$ is associated with the dominant contribution to the stellar deformation, while the tidal deformability describes the ratio of each star's induced mass quadrupole moment to the tidal field of its companion [29,31,32]. They are related by,

$$\Lambda = \frac{2}{3} k_2 \left(\frac{R}{M}\right)^5. \tag{15}$$

In order to calculate the tidal deformability with our EOS table, we should solve the Tolman-Oppenheimer-Volkoff equations

$$\frac{\mathrm{d}P(r)}{\mathrm{d}r} = -\frac{(\epsilon + P)(M + 4\pi r^3 P)}{r(r - 2M)}, \tag{16}$$

$$\frac{\mathrm{d}M(r)}{\mathrm{d}r} = 4\pi r^2 \epsilon, \tag{17}$$

simultaneously with

$$\frac{\mathrm{d}H(r)}{\mathrm{d}r} = \beta, \tag{18}$$

$$\begin{aligned}\frac{\mathrm{d}\beta(r)}{\mathrm{d}r} = {} & 2\left(1-2\frac{M}{r}\right)^{-1} H\left\{-2\pi[5\epsilon + 9P + f(\epsilon + P)]\right. \\ & \left. + \frac{3}{r^2} + 2\left(1-2\frac{M}{r}\right)^{-1}\left(\frac{M}{r^2} + 4\pi r P\right)^2\right\} \\ & + \frac{2\beta}{r}\left(1-2\frac{M}{r}\right)^{-1}\left\{-1 + \frac{M}{r} + 2\pi r^2(\epsilon - P)\right\},\end{aligned} \tag{19}$$

where $f$ is given by

$$f = \frac{\mathrm{d}\epsilon}{\mathrm{d}P} \tag{20}$$

for slow changes in matter configurations. Equations (18) and (19) are integrated outward starting just outside the center via the expansions: $H(r) = a_0 r^2$, and $\beta(r) = 2a_0 r$ as $r \to 0$, where $a_0$ is a constant which determines how much the star is deformed by an external tidal field and can be chosen arbitrarily as it cancels in the expression for the Love number $k_2$. Hence, in our calculations, we choose $a_0 = 1$ for simplicity.

For the internal solution, the $l = 2$ tidal Love number $k_2$ is

$$\begin{aligned}k_2 = {} & \frac{8C^5}{5}(1-2C)^2[2 + 2C(y_R - 1) - y_R] \\ & \times \{2C[6 - 3y_R + 3C(5y_R - 8)] \\ & + 4C^3[13 - 11y_R + C(3y_R - 2) + 2C^2(1 + y_R)] \\ & + 3(1-2C)^2[2 - y_R + 2C(y_R - 1)]\ln(1-2C)\}^{-1},\end{aligned} \tag{21}$$

where $C = M/R$ is the compactness of the star, and $y_R = y(R) = [r\beta(r)/H(r)]_{r=R}$.

As discussed in Refs. [33,34], if there is a first-order hadron-quark phase transition in the EOS, there is a jump of $\Delta\epsilon$ in the energy density at constant pressure $P_{\mathrm{tr}}$, hence this delta-function behavior should be added in Eq. (20) as

$$f = \left.\frac{\mathrm{d}\epsilon}{\mathrm{d}P}\right|_{P \neq P_{\mathrm{tr}}} + \delta(P - P_{\mathrm{tr}})\Delta\epsilon. \tag{22}$$

This leads to an extra term for the solution of $y(r)$ across $r_{\mathrm{tr}}$, which is given by

$$y(r_{\mathrm{tr}}^+) - y(r_{\mathrm{tr}}^-) = -\frac{4\pi r_{\mathrm{tr}}^3 \Delta\epsilon}{M(r_{\mathrm{tr}}) + 4\pi r_{\mathrm{tr}}^3 P(r_{\mathrm{tr}})}, \tag{23}$$

where $r_{\mathrm{tr}}$ is the position where this first-order hadron-quark phase transition happens, $\Delta\epsilon = \epsilon(r_{\mathrm{tr}}^-) - \epsilon(r_{\mathrm{tr}}^+)$, and $r_{\mathrm{tr}}^{\pm} = r_{\mathrm{tr}} \pm \delta r$ where $\delta r$ is an infinitesimal distance around $r_{\mathrm{tr}}$.

For strange quark stars, since there is a finite energy density discontinuity in the vicinity of the surface $R$, we should also add this extra term to $y(R)$ and we obtain

$$y_R = \frac{R\beta(R)}{H(R)} - \frac{4\pi R^3 \Delta\epsilon}{M + 4\pi R^3 P(R)}. \quad (24)$$

Here $\Delta\epsilon = \epsilon(R^-)$ is the energy density just inside the surface, and the pressure at the surface is given by $P(R) = 0$.

The parameters are set up in the following ways. $\zeta$ is changing from 0.05 GeV to 0.095 GeV, for in this region the running coupling constant $\alpha_s(\mu)$ varies consistent with the experimental data [35]. The vacuum pressure $B$ varies from $(0.098\ \mathrm{GeV})^4$ to $(0.148\ \mathrm{GeV})^4$, which ensures the surface energy density is always larger than $2.80\times10^{14}\,\mathrm{g\,cm^{-3}}$. The mass of $u$ or $d$ quark is very small, and we set $m_{u0} = m_{d0} = 0$ MeV. The mass of $s$ quark varies from 0 MeV to 120 MeV.

In all the figures of this paper, the results are presented in three represented colors (cyan, blue and red). The quantities shown in cyan represent the results calculated from the EOSs with the maximum strange quark star mass smaller than $2.0M_\odot$, while the quantities shown in blue represent the results calculated from the EOSs with the maximum strange quark star mass larger than $2.0M_\odot$ and the tidal deformability for a 1.4 $M_\odot$ strange quark star smaller than 800, and the quantities shown in red exhibit the results calculated from the EOSs with the maximum strange quark star mass larger than $2.0M_\odot$ but the tidal deformability for a $1.4M_\odot$ strange quark star larger than 800.

The equations of state are displayed in Fig. 1. The gray-dashed line stands for $P = \epsilon$. We can see from this picture that the mass constraint $2.0M_\odot$ from the observables PSR J1614-2230 ($M = 1.928 \pm 0.017M_\odot$ [11]) and PSR J0348 + 0432 ($M = 2.01 \pm 0.04M_\odot$ [10]) rules out the EOSs that are soft at low densities, and the constraint on the tidal deformability of $\Lambda_{1.4} < 800$ from GW170817 [12] rules out the EOSs that are too stiff in the low density region. These conclusions are consistent with the cases of neutron star EOSs [36].

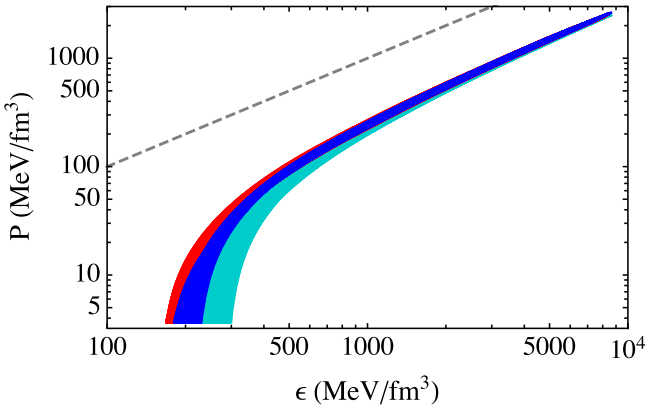


FIG. 1. Equations of state for strange quark stars. The gray-dashed line stands for $P = \epsilon$.

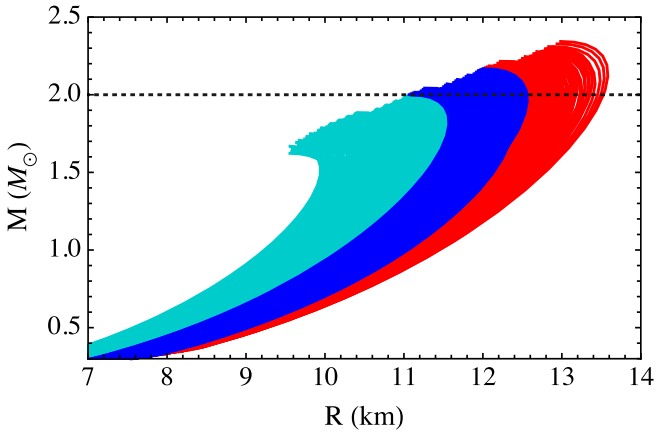


FIG. 2. Mass-radius relations for strange quark stars. The black-dotted line stands for $M = 2.0\ M_\odot$.

The mass-radius relations for strange quark stars are shown in Fig. 2. The black-dotted line stands for $M = 2.0M_\odot$.

The astrophysically compatible EOSs (the blue-solid lines) are selected by the constraints of $M_{\mathrm{TOV}} > 2.0M_\odot$ and $\Lambda_{1.4} < 800$, where $M_{\mathrm{TOV}}$ is the maximum mass of the solution of TOV equations. There are many reasonable parameters that can fullfill these two astrophysical constraints. For definite $\zeta$ and $m_{s0}$ the upper limit of $B$ is determined by the mass constraint while the lower limit of $B$ is determined by the constraint of $\Lambda_{1.4} < 800$. For instance, for $\zeta = 0.05$ GeV and $m_{s0} = 90$ MeV, the astrophysically compatible EOSs are obtained for $(0.130\ \mathrm{GeV})^4 \lesssim B \lesssim (0.133\ \mathrm{GeV})^4$. For larger values of $\zeta$ or with increasing $m_{s0}$, both upper and lower limits of $B$ are shifted to lower values.

Assuming low spin priors for the two compact stars in the analysis of GW170817 [12], the component masses are $m_1 \in [1.36, 1.60]M_\odot$ and $m_2 \in [1.16, 1.36]M_\odot$. The range of the radius of a $1.36M_\odot$ strange quark star obtained by the astrophysically compatible EOSs is $11.04\ \mathrm{km} < R_{1.36} < 11.91\ \mathrm{km}$, while for the neutron star EOSs, a $1.36M_\odot$ neutron star has a radius of 10.4 km (WFF1), 11.3 km (APR4), 11.7 km (SLy), 12.4 km (MPA1), 14.0 km (H4), 14.5 km (MS1b), and 14.9 km (MS1) [37]. These radii are similar to our results, except that the last three EOSs (H4, MS1b, MS1) lying outside of the 90% credible region of GW170817 give much larger radii. The range of the radius of a $1.16M_\odot$ strange quark star calculated by the astrophysically compatible EOSs is $10.62\mathrm{km} < R_{1.16} < 11.48\ \mathrm{km}$, and the range of the radius of a $1.6M_\odot$ strange quark star obtained by the astrophysically compatible EOSs is $11.42\ \mathrm{km} < R_{1.6} < 12.26\ \mathrm{km}$. These results show a little bit narrower range of the radius of strange quark stars across all mass priors in GW170817 than that in Ref. [38] where they have found a robust measurement of the common radius of the neutron stars across all mass priors

of $8.9 \leq R \leq 13.2$ km with a mean value of $\langle R \rangle = 10.8$ km. Also, the LIGO and Virgo collaboration [39] measure the two neutron star radii as $R_1 = 10.8^{+2.0}_{-1.7}$ km for the heavier star and $R_2 = 10.7^{+2.1}_{-1.5}$ km for the lighter star at the 90% credible level, which covers our ranges for the radii of the two compact stars.

Assuming low spin priors for the two compact stars in the analysis of GW190425 [40], the component masses are $m_1 \in [1.60, 1.87]M_\odot$ and $m_2 \in [1.46, 1.69]M_\odot$. And our results show that the range of the radius of a $1.46M_\odot$ strange quark star is 11.22 km $< R_{1.46} <$ 12.07 km, the range of the radius of a $1.69M_\odot$ strange quark star is 11.51 km $< R_{1.69} <$ 12.35 km, and the range of the radius of a $1.87M_\odot$ strange quark star is 11.56 km $< R_{1.87} <$ 12.53 km.

Among the results obtained from the astrophysically compatible EOSs, the lowest maximum mass 2.0 $M_\odot$ corresponds to $R_{2.0} = 11.07$ km, while the largest maximum mass is 2.17 $M_\odot$ that corresponds to $R_{2.17} = 12.00$ km. The range for the radius of a $1.4M_\odot$ strange quark star is 11.12 km $< R_{1.4} <$ 11.98 km, which is consistent with that obtained in Ref. [41]. In that article, the authors construct the equations of state constrained by chiral effective field theory and marginalized over these using the gravitational-wave observations. Combining this with the electromagnetic observations of the merger remnant that imply the presence of a short-lived hypermassive neutron star, they find that the radius of a $1.4M_\odot$ neutron star is $R_{1.4} = 11.0^{+0.9}_{-0.6}$ km (90% credible interval).

The lower bound of $\Lambda_{1.4} > 513.66$ is also obtained for a $1.4M_\odot$ strange quark star from the astrophysically compatible EOSs, which is similar to the result of $\Lambda_{1.4} > 510.058$ inferred from Eq. (3) in Ref. [2] using the MIT bag model.

Figure 3 shows the correlation between the tidal deformablity and the radius, both of which are calculated for strange quark stars with 1.4 $M_\odot$. The purple-solid line stands for the empirical function $\Lambda_{1.4} = 2.86 \times 10^{-5}(R/\mathrm{km})^{6.92}$ in this work, while the other solid lines show the empirical functions for model calculations of neutron stars. The blue-solid line is the empirical function of $\Lambda_{1.4} = 2.88 \times 10^{-6}(R/\mathrm{km})^{7.5}$ from Ref. [36] using a family of EOSs constructed that interpolate between a chiral effective theory EOS below saturation density and a perturbative QCD EOS at high densities. The green-solid line stands for the empirical function of $\Lambda_{1.4} = 1.53 \times 10^{-5}(R/\mathrm{km})^{6.83}$ from Ref. [42] analyzing a fully comprehensive set of relativistic nuclear mean field theories. The red-solid line is the empirical function of $\Lambda_{1.4} = 1.41 \times 10^{-6}(R/\mathrm{km})^{7.71}$ from Ref. [43] using the EOS of symmetric nuclear matter. And the magenta-solid line shows the empirical function of $\Lambda_{1.4} = 5.22 \times 10^{-5}(R/\mathrm{km})^{6.35}$ from Ref. [44] via several nucleonic EOSs with a nucleon-quark phase transition.

For neutron stars, the LIGO-Virgo measurement can give a limit of radii via the correlation functions. The 90% limit

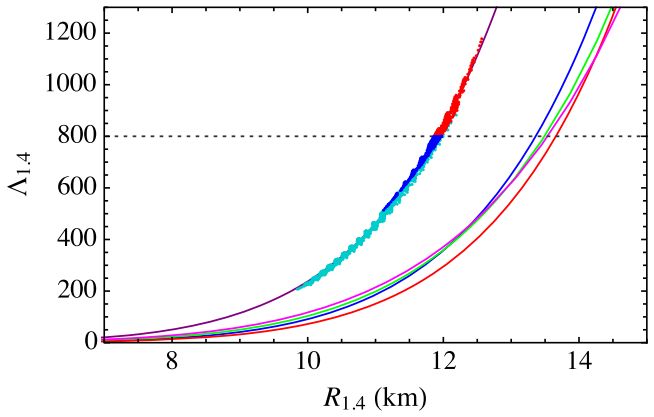


FIG. 3. Λ-R correlation for 1.4 $M_\odot$ strange quark stars. The purple-solid line stands for the empirical function in this work: $\Lambda_{1.4} = 2.86 \times 10^{-5}(R/\mathrm{km})^{6.92}$. The other lines show the empirical functions for model calculations of neutron stars: $\Lambda_{1.4} = 2.88 \times 10^{-6}(R/\mathrm{km})^{7.5}$ (the blue-solid line), $\Lambda_{1.4} = 1.53 \times 10^{-5}(R/\mathrm{km})^{6.83}$ (the green-solid line), $\Lambda_{1.4} = 1.41 \times 10^{-6}(R/\mathrm{km})^{7.71}$ (the red-solid line), and $\Lambda_{1.4} = 5.22 \times 10^{-5}(R/\mathrm{km})^{6.35}$ (the magenta-solid line).

of $\Lambda_{1.4} < 800$ lead to an upper limit of $R_{1.4} < 13.6$ km (the blue-solid line), $R_{1.4} < 13.49$ km (the green-solid line), $R_{1.4} < 13.66$ km (the red-solid line), $R_{1.4} < 13.54$ km (the magenta-solid line).

For strange quark stars, $\Lambda_{1.4}$ also exhibits a very strong correlation with $R_{1.4}$, and it is natural that strange quark stars with larger radius have larger Λ, for Λ quantifies the deformation of the stellar gravitational field from that of a point-like object. Obviously, the Λ-R correlation of strange quark stars is quite different from that of neutron stars. The tidal deformabilities of $1.4M_\odot$ strange quark stars are larger than that of the neutron stars with the same radius. The reason is that there is finite large energy density at the surface of strange quark stars, which makes the $y$ term of strange quark stars in Eq. (21) much smaller than that of neutron stars, see Eq. (24), and ends up to $k_2$ of strange quark stars much larger than that of neutron stars. This feature might be used to distinguish strange quark stars from neutron stars.

We now consider the combined tidal deformabilities of two compact stars in the binary inspiral. For the chirp mass enters the phase evolution at the lowest order, it is the best measured parameter for systems displaying a long inspiral, which reads

$$\mathcal{M} = \frac{(m_1 m_2)^{3/5}}{(m_1 + m_2)^{1/5}}, \tag{25}$$

where $m_1$ and $m_2$ are the masses of the two compact stars. And to the leading order in tidal deformabilities, the gravitational-wave phase is determined by the combination:

$$\tilde{\Lambda} = \frac{16}{13}\frac{(m_1 + 12m_2)m_1^4\Lambda_1 + (m_2 + 12m_1)m_2^4\Lambda_2}{(m_1 + m_2)^5}, \tag{26}$$

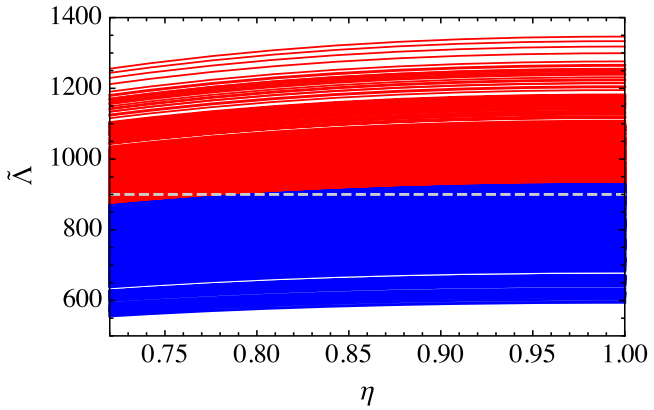


FIG. 4. Combined tidal deformability $\tilde{\Lambda}$ as a function of $\eta$ calculated for the case of GW170817 by the EOSs with $M_{\rm TOV} > 2.0\ M_\odot$. The gray-dashed line stands for $\tilde{\Lambda} = 900$.

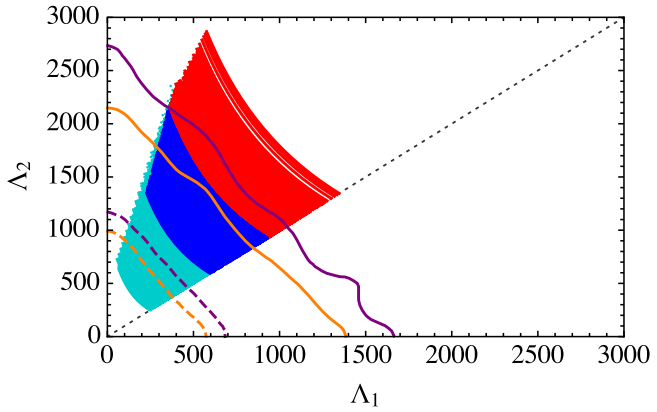


FIG. 5. $(\Lambda_1, \Lambda_2)$ obtained for the case of GW170817. The purple-dashed line and the purple-solid line stand for the 50% and 90% probability contours given in Fig. 5 of Ref. [12], respectively. The orange-dashed line and the orange-solid line represent the 50% and 90% probability contours given in Fig. 10 of Ref. [37], respectively.

where $\Lambda_1$ and $\Lambda_2$ are the tidal deformabilities of the two compact stars.

Assuming low spin priors for the two compact stars in the analysis of GW170817 [12], the chirp mass is $\mathcal{M} = 1.186^{+0.001}_{-0.001}\ M_\odot$, the component masses are $m_1 \in [1.36, 1.60]\ M_\odot$ and $m_2 \in [1.16, 1.36]\ M_\odot$, and the mass ratio is $\eta = m_2/m_1 \in [0.72, 1.0]$.

We can see clearly from Fig. 4 that the combined tidal deformability $\tilde{\Lambda}$ is a monotonically increasing function of the mass ratio $\eta$, but the slope is very small. The ratio of $\tilde{\Lambda}|_{\eta=0.72}$ to $\tilde{\Lambda}|_{\eta=1.0}$ is about $93.38\% \sim 93.58\%$. For $\mathcal{M} = 1.186$, when $\eta = 1.0$, one can get $m_1 = m_2 = 2^{1/5}\mathcal{M} = 1.36 M_\odot$, hence, $\tilde{\Lambda}$ should be smaller than $\Lambda|_{m=1.36\ M_\odot}$. This conclusion is very useful for us to predict the upper bound of $\tilde{\Lambda}$ in the case of GW190425. All of the $\tilde{\Lambda}$s calculated by the astrophysically compatible EOSs here are staying below the upper bound of $\tilde{\Lambda} < 900$ (90% credible interval) [37].

The two tidal parameters $\Lambda_1$ and $\Lambda_2$ are also shown in Fig. 5 with the 50% and 90% probability contours for the tidal deformabilities of the two stars measured by LIGO and Virgo. The purple-dashed line and the purple-solid line stand for the 50% and 90% probability contours given in Fig. 5 of Ref. [12], respectively. The orange-dashed line and the orange-solid line represent the 50% and 90% probability contours given in Fig. 10 of Ref. [37], respectively. Both of them are for the waveform models of TaylorF2. The orange lines are calculated using a lower starting frequency of 23 Hz instead of 30 Hz, resulting in the upper bounds of $\Lambda_1$ and $\Lambda_2$ are about 20% smaller than the purple lines. All of the astrophysically compatible EOSs stay inside of the 90% probability contour from Ref. [12], while more than half of the astrophysically compatible EOSs stay inside of the 90% probability contour from Ref. [37].

Assuming low spin priors for the two compact stars in the analysis of GW190425 [40], the chirp mass is $\mathcal{M} = 1.44^{+0.02}_{-0.02} M_\odot$, the component masses are $m_1 \in [1.60, 1.87] M_\odot$ and $m_2 \in [1.46, 1.69] M_\odot$, and the mass ratio is $\eta = m_2/m_1 \in [0.8, 1.0]$. The combined tidal deformabilities $\tilde{\Lambda}$s as a function of mass ratio $\eta$ are shown in Fig. 6. Here, the ratio of $\tilde{\Lambda}|_{\eta=0.8}$ to $\tilde{\Lambda}|_{\eta=1.0}$ is about $96.48\% \sim 96.95\%$, which is larger than that in the case of GW170817. Hence the difference between $\tilde{\Lambda}|_{\eta=0.8}$ and $\tilde{\Lambda}|_{\eta=1.0}$ is smaller than that in the case of GW170817. For $\mathcal{M} = 1.44$, when $\eta = 1.0$, one can obtain $m_1 = m_2 = 2^{1/5}\mathcal{M} = 1.65 M_\odot$, hence, $\tilde{\Lambda}$ should be smaller than $\Lambda|_{m=1.65\ M_\odot}$. The upper bound of $\tilde{\Lambda}$ can be obtained by calculating the maximum value when $\eta = 1.0$, while the lower bound of $\tilde{\Lambda}$ can be obtained by calculating the minimum value when $\eta = 0.8$. Finally, we can obtain that the range of $\tilde{\Lambda}$ calculated from the astrophysically

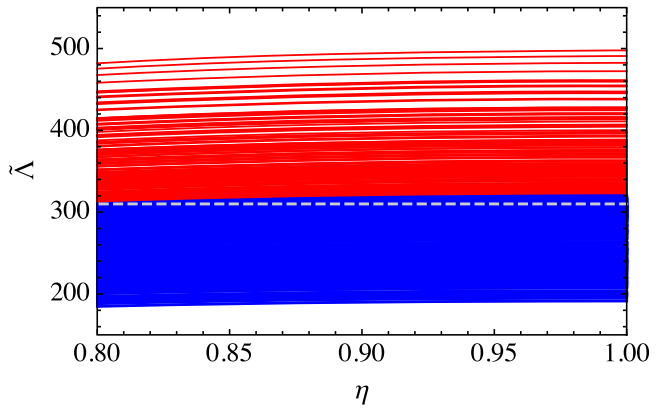


FIG. 6. Combined tidal deformability $\tilde{\Lambda}$ as a function of $\eta$ calculated for the case of GW190425 by the EOSs with $M_{\rm TOV} > 2.0\ M_\odot$. The gray-dashed line stands for $\tilde{\Lambda} = 310.05$, which is the maximum value when $\eta = 0.8$.

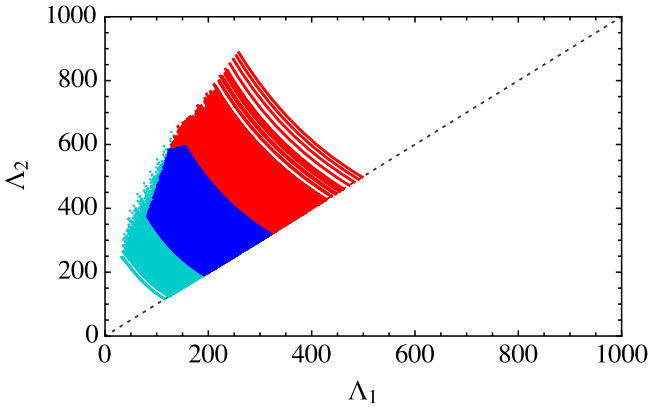


FIG. 7. $(\Lambda_1, \Lambda_2)$ obtained for the case of GW190425.

compatible EOSs for GW190425 is $184.81 < \tilde{\Lambda} < 320.08$, which satisfies the constraint $\tilde{\Lambda} < 600$ that reported in Ref. [40]. The two tidal parameters $\Lambda_1$ and $\Lambda_2$ are also shown in Fig. 7.

## IV. SUMMARY

The tidal deformabilities and radii of strange quark stars are calculated via the quasiparticle model which includes the nonperturbative features of QCD in the low-density region. Our results show that the mass constraint $2.0M_\odot$ rules out the EOSs which are soft at low densities, while the constraint on the tidal deformability of $\Lambda_{1.4} < 800$ rules out the EOSs which are too stiff in the low density region.

The ranges of the radii of 1.36 $M_\odot$, 1.16 $M_\odot$, and $1.6M_\odot$ strange quark star are $11.04\ \text{km} < R_{1.36} < 11.91\ \text{km}$, $10.62\,\text{km} < R_{1.16} < 11.48\,\text{km}$, and $11.42\ \text{km} < R_{1.6} < 12.26\ \text{km}$, respectively. These results show a little bit narrower range of the radius of strange quark stars across all mass priors in GW170817 than that given in Ref. [38]. And our results also show that the ranges of the radii of $1.46M_\odot$, $1.69M_\odot$, and $1.87M_\odot$ (mass bounds in GW190425) strange quark star are $11.22\ \text{km} < R_{1.46} < 12.07\ \text{km}$, $11.51\ \text{km} < R_{1.69} < 12.35\ \text{km}$, and $11.56\ \text{km} < R_{1.87} < 12.53\ \text{km}$, respectively.

$\Lambda_{1.4}$ has a strong correlation with $R_{1.4}$ for strange quark stars, and the empirical correlation function is $\Lambda_{1.4} = 2.86 \times 10^{-5}(R/\text{km})^{6.92}$. The range for the radius of a $1.4M_\odot$ strange quark star is $11.12\,\text{km} < R_{1.4} < 11.98\,\text{km}$. $\Lambda_{1.4}$ of strange quark stars is much larger than that of neutron star with the same radius, for there is finite large energy density at the surface of strange quark stars. This feature could be used to distinguish strange quark stars from neutron stars. The lower bound of $\Lambda_{1.4} > 513.66$ is also obtained for strange quark stars.

$\tilde{\Lambda}$ is a monotonically increasing function of $\eta$, but the slope is very small. Assuming low spin priors for the two compact stars in the analysis of GW170817, the ratio of $\tilde{\Lambda}|_{\eta=0.72}$ to $\tilde{\Lambda}|_{\eta=1.0}$ is about $93.38\% \sim 93.58\%$ and $\tilde{\Lambda}$ should be smaller than $\Lambda|_{m=1.36M_\odot}$. All of the $\tilde{\Lambda}$s calculated by the astrophysically compatible EOSs are staying below the upper bound of $\tilde{\Lambda} < 900$ (90% credible interval). The two tidal parameters $\Lambda_1$ and $\Lambda_2$ are also shown in Fig. 5 with the 50% and 90% probability contours for the tidal deformabilities of the two stars measured by LIGO and Virgo. All of the astrophysically compatible EOSs stay inside of the 90% probability contour from Ref. [12], while more than half of the astrophysically compatible EOSs stay inside of the 90% probability contour from Ref. [37].

Assuming low spin priors for the two compact stars in the analysis of GW190425, the ratio of $\tilde{\Lambda}|_{\eta=0.8}$ to $\tilde{\Lambda}|_{\eta=1.0}$ is about $96.48\% \sim 96.95\%$, which is larger than that in the case of GW170817. The difference between $\tilde{\Lambda}|_{\eta=0.8}$ and $\tilde{\Lambda}|_{\eta=1.0}$ is smaller than that in the case of GW170817. and $\tilde{\Lambda}$ should be smaller than $\Lambda|_{m=1.65M_\odot}$. The range of $\tilde{\Lambda}$ for GW190425 obtained from the astrophysically compatible EOSs is $184.81 < \tilde{\Lambda} < 320.08$. The two tidal parameters $\Lambda_1$ and $\Lambda_2$ are also shown in Fig. 7.

While studying a strange quark star composed of $u$, $d$, and $s$ quarks, if the number densities of the three quarks satisfy $\rho_u = \rho_d = \rho_s$, then this strange quark star is electrically neutral. Actually, for the mass of $s$ quark is larger than that of $u$ and $d$ quarks, the electrons should come up with number density $\rho_e = \alpha(\rho_u + \rho_d + \rho_s)$ where $\alpha \simeq 10^{-5} \sim 10^{-4}$. The Fermi energy of the electrons is smaller than the mass of muon, and the number density of leptons is very small. Hence, even if we include muons at high energy density, the picture we discussed in this paper will not change.

## ACKNOWLEDGMENTS

This work is supported by the National Natural Science Foundation of China (under Grants No. 11805097, No. 11775118, and No. 11535005), the Jiangsu Provincial Natural Science Foundation of China (under Grant No. BK20180323), the China Postdoctoral Science Foundation (under Grant No. 2020M681655), and the Jiangsu Planned Projects for Postdoctoral Research Funds (under Grants No. 2020Z271).

[1] G. Baym, T. Hatsuda, T. Kojo, P. D. Powell, Y. Song, and T. Takatsuka, Rep. Prog. Phys. **81**, 056902 (2018).
[2] E.-P. Zhou, X. Zhou, and A. Li, Phys. Rev. D **97**, 083015 (2018).
[3] D. P. Menezes, C. Providncia, and D. B. Melrose, J. Phys. G **32**, 1081 (2006).
[4] C. Alcock, E. Farhi, and A. Olinto, Astrophys. J. **310**, 261 (1986).
[5] M. Alford, M. Braby, M. Paris, and S. Reddy, Astrophys. J. **629**, 969 (2005).
[6] A. Li, Z.-Y. Zhu, and X. Zhou, Astrophys. J. **844**, 41 (2017).
[7] A. Peshier, B. Kämpfer, and G. Soff, Phys. Rev. C **61**, 045203 (2000).
[8] B.-L. Li, Z.-F. Cui, Z.-H. Yu, Y. Yan, S. An, and H.-S. Zong, Phys. Rev. D **99**, 043001 (2019).
[9] Y. Yan, J. Cao, X.-L. Luo, W.-M. Sun, and H. Zong, Phys. Rev. D **86**, 114028 (2012).
[10] J. Antoniadis, P. C. C. Freire, N. Wex, T. M. Tauris, R. S. Lynch, M. H. van Kerkwijk, M. Kramer, C. Bassa, V. S. Dhillon, T. Driebe, J. W. T. Hessels, V. M. Kaspi, V. I. Kondratiev, N. Langer, T. R. Marsh, M. A. McLaughlin, T. T. Pennucci, S. M. Ransom, I. H. Stairs, J. van Leeuwen, J. P. W. Verbiest, and D. G. Whelan, Science **340**, 1233232 (2013).
[11] E. Fonseca, T. T. Pennucci, J. A. Ellis, I. H. Stairs, D. J. Nice, S. M. nsom, P. B. Demorest, Z. Arzoumanian, K. Crowter, T. Dolch, R. D. Ferdman, M. Gonzalez, G. Jones, M. L. Jones, M. T. Lam, L. Levin, M. A. McLaughlin, K. Ovall, J. K. Swiggum, and W. Zhu, Astrophys. J. **832**, 167 (2016).
[12] B. P. Abbott, R. Abbott, T. D. Abbott, F. Acernese, K. Ackley, C. Adams, T. Adams, P. Addesso *et al.* (LIGO Scientific and Virgo Collaborations), Phys. Rev. Lett. **119**, 161101 (2017).
[13] A. Peshier, B. Kampfer, O. Pavlenko, and G. Soff, Phys. Lett. B **337**, 235 (1994).
[14] M. I. Gorenstein and S. N. Yang, Phys. Rev. D **52**, 5206 (1995).
[15] H.-S. Zong and W.-M. Sun, Int. J. Mod. Phys. A **23**, 3591 (2008).
[16] A.-M. Zhao, J. Cao, L.-J. Luo, W.-M. Sun, and H.-S. Zong, Mod. Phys. Lett. A **25**, 47 (2010).
[17] P. Lévai and U. Heinz, Phys. Rev. C **57**, 1879 (1998).
[18] V. M. Bannur, Phys. Rev. C **78**, 045206 (2008).
[19] V. M. Bannur, Phys. Rev. C **75**, 044905 (2007).
[20] W. E. Caswell, Phys. Rev. Lett. **33**, 244 (1974).
[21] H.-s. Zong and W.-m. Sun, Phys. Rev. D **78**, 054001 (2008).
[22] M. A. Halasz, A. D. Jackson, R. E. Shrock, M. A. Stephanov, and J. J. M. Verbaarschot, Phys. Rev. D **58**, 096007 (1998).
[23] M. He, W.-m. Sun, H.-t. Feng, and H.-s. Zong, J. Phys. G **34**, 2655 (2007).
[24] J. I. Kapusta and C. Gale, *Finite-Temperature Field Theory: Principles and Applications*, 2nd ed., Cambridge Monographs on Mathematical Physics (Cambridge University Press, Cambridge, England, 2006).
[25] E. E. Flanagan and T. Hinderer, Phys. Rev. D **77**, 021502 (2008).
[26] T. Hinderer, Astrophys. J. **677**, 1216 (2008).
[27] T. Hinderer, Astrophys. J. **697**, 964 (2009).
[28] T. Hinderer, B. D. Lackey, R. N. Lang, and J. S. Read, Phys. Rev. D **81**, 123016 (2010).
[29] T. Damour and A. Nagar, Phys. Rev. D **80**, 084035 (2009).
[30] K. Yagi and N. Yunes, Science **341**, 365 (2013).
[31] T. Damour, M. Soffel, and C. Xu, Phys. Rev. D **45**, 1017 (1992).
[32] T. Binnington and E. Poisson, Phys. Rev. D **80**, 084018 (2009).
[33] S. Postnikov, M. Prakash, and J. M. Lattimer, Phys. Rev. D **82**, 024016 (2010).
[34] J. Takátsy and P. Kovács, Phys. Rev. D **102**, 028501 (2020).
[35] S. Bethke, Prog. Part. Nucl. Phys. **58**, 351 (2007).
[36] E. Annala, T. Gorda, A. Kurkela, and A. Vuorinen, Phys. Rev. Lett. **120**, 172703 (2018).
[37] B. P. Abbott, R. Abbott, T. D. Abbott, F. Acernese, K. Ackley, C. Adams, T. Adams, P. Addesso *et al.* (LIGO Scientific and Virgo Collaborations), Phys. Rev. X **9**, 011001 (2019).
[38] S. De, D. Finstad, J. M. Lattimer, D. A. Brown, E. Berger, and C. M. Biwer, Phys. Rev. Lett. **121**, 091102 (2018).
[39] B. P. Abbott, R. Abbott, T. D. Abbott, F. Acernese, K. Ackley, C. Adams, T. Adams, P. Addesso *et al.* (The LIGO Scientific and the Virgo Collaborations), Phys. Rev. Lett. **121**, 161101 (2018).
[40] B. P. Abbott, R. Abbott, T. D. Abbott, F. Acernese, K. Ackley, C. Adams, T. Adams, P. Addesso *et al.* (LIGO Scientific and Virgo Collaborations), Astrophys. J. **892**, L3 (2020).
[41] C. D. Capano, I. Tews, S. M. Brown, B. Margalit, S. De, S. Kumar, D. A. Brown, B. Krishnan, and S. Reddy, Nat. Astron. **4**, 625 (2020).
[42] R. Nandi, P. Char, and S. Pal, Phys. Rev. C **99**, 052802 (2019).
[43] Y. Zhou, L.-W. Chen, and Z. Zhang, Phys. Rev. D **99**, 121301 (2019).
[44] R. Nandi and S. Pal, Eur. Phys. J. Spec. Top. **230**, 551 (2021).